IEEE Access
Multidisciplinary | Rapid Review | Open Access Journal

Received January 10, 2019, accepted January 19, 2019, date of publication January 31, 2019, date of current version March 29, 2019.

Digital Object Identifier 10.1109/ACCESS.2019.2895960

Novel Optimization Approach in Ultrasonic Machining: Unilateral Compensation for Resonant Vibration in Primary Side

JIANGUO ZHANG[1], ZHILI LONG[1,2], (Member, IEEE), CAN WANG[1], (Member, IEEE), FENG REN[1], AND YANGMING LI[3], (Senior Member, IEEE)

[1]Department of Mechanical Engineering, Harbin Institute of Technology, Shenzhen 518055, China
[2]Key Laboratory of Precision Microelectronic Manufacturing Technology & Equipment, Ministry of Education, Guangdong University of Technology, Guangzhou, China
[3]Department of Industrial and Systems Engineering, The Hong Kong Polytechnic University, Hong Kong

Corresponding author: Zhili Long (longzhili@hit.edu.cn)

This work was supported in part by the National Natural Science Foundation of China under Grant U1713206, in part by the Basic Research Plan of Shenzhen under Grant JCYJ20170413112645981, and in part by the Shenzhen Technology Innovation Program under Grant JCYJ20170811160003571.

ABSTRACT Resonant frequency and impedance matching have great significance for the vibration performance and online monitoring of the rotary ultrasonic machining. Network compensation is a typical solution to match the resonant frequency and the impedance between the rotary ultrasonic holder (RUH) and the ultrasonic transducer. However, the traditional bilateral compensation method could adversely affect the rotary dynamic balance of the RUH. Currently, the existing unilateral compensation methods can only realize the resonant frequency matching. A novel unilateral compensation method that satisfies both the resonant frequency and the impedance matching is proposed. First, the impedance model of the RUH vibrating system is established according to its equivalent circuit. It is found that, without any compensation methods, the resonant frequency and the impedance between the RUH and the transducer have deviated. Second, the primary-series and primary-parallel compensation topologies are applied to the RUH system, and the expressions of compensation capacitance value, voltage gain, power transfer efficiency, and output active power are derived. The deviations of the resonant frequency and the impedance are eliminated with primary-series compensation topology; and as a result, the voltage gain is increased from 0.267 to 0.90, the output active power is 11.3 times than that without compensation. Third, the state-space model of primary-series topology is constructed. Finally, the above theoretical results are verified by the experimental results.

INDEX TERMS Unilateral compensation, resonant frequency, impedance matching, contactless rotary transformer, rotary ultrasonic machining.

I. INTRODUCTION

Hard and brittle materials, with the advantages of high hardness, incompressibility, wear resistance and low density, have been widely applied to automobile, medical devices and aerospace equipment. These typical materials include quartz, ferrite, industrial diamond, SiC, and advanced ceramics etc. [1], [2]. Unfortunately, due to their high hardness and brittleness, conventional machining methods such as diamond abrasive grinding cannot process them efficiently. Many untraditional machining methods, including abrasive water jet machining, laser beam machining, and rotary ultrasonic machining (RUM) are invented to improve the machining efficiency [2]. Currently, RUM has become one of the dominant technologies for machining hard-brittle materials, because it not only reduces cutting force, improves surface quality and reduces tool wear, but also increases machining efficiency [3]–[6].

The RUH vibrating system in RUM consists of an electrical power driver, a pair of contactless rotary transformer and an ultrasonic piezoelectric transducer. The electrical power driver is a key electronic module, which provides high-power voltage, automatic resonant frequency tracking ability and online machining process monitoring ability. The contactless

The associate editor coordinating the review of this manuscript and approving it for publication was Yingxiang Liu.

rotary transformer is an electromagnetic induction component composed of a static primary side and a dynamic secondary side, where the electric energy can be transmitted from the electric driver to the secondary side through the air-gap by the mutual inductance. The ultrasonic transducer is an actuator component that converts AC electric power into mechanical vibration to accelerate the removal of the hard and brittle materials [7], [8]. Generally, the output amplitude of ultrasonic transducer varies drastically with the driving frequency, and the maximum vibration amplitude can be achieved when it operates at the mechanical resonant frequency [9]. Therefore, the resonant frequency of the RUH should match with that of the transducer. Furthermore, since the RUH vibrating system is sensitive to the machining force, the machining process can be monitored by the impedance or electric current of the RUH and transducer. As a result, resonant frequency and impedance matching of the RUH vibrating system are the current emphasis to investigate.

The optimizations of RUH vibrating system to improve the vibration performance have drawn interests and attention from many researchers [10]–[12]. The sufficient output power capability of rotary transformers is crucial to ensure the transducer to vibrate efficiently. Brotis *et al.* [13] proposed the LLCC-filter to enable the proper and robust operation of the rotary machining system. Zhu *et al.* [14], [15] presented the mathematical models to calculate bilateral compensation capacitance values, and proved that the compensation topology can improve the power transfer efficiency. Although above literatures have improved the output power capability of the contactless transformer, they are bilateral optimization structure. That is to say, the compensation method has to be applied in both the primary and secondary side. However, the secondary compensation element needs to be mounted in the very compact RUH mechanical structure, which is difficult to realize. Moreover, when the dynamic part of RUH rotates with high speed, a large centrifugal force will be generated, which would not only be a great challenge for the stable installation of the compensation elements in secondary side but also troubles the rotary dynamic balance of RUH vibrating system. In order to solve the problems of the bilateral compensation, some effective solutions are proposed. J. Imaoka investigated primary side series-parallel combined resonant circuit with asymmetric rotary transformers used for the ultrasonic spindle drive. The proposed method contributes to reduce the voltage drop caused by the leakage inductances and improves the primary side power factor even if the resonance parameter has the error or the frequency of input voltage changes in wide frequency ranges [16], [17]. Liu *et al.* [18] proposed a primary compensation method to match the power supply's internal impedance and get high transfer efficiency by optimizing the coils ratio. Jiang *et al.* investigated the self-compensation theory that can overcome the shortcomings of bilateral compensation. The secondary leakage inductance of the rotary transformers can be compensated by static capacitance of the transducer [19]. At present, various unilateral compensation methods are proposed, however, the impedance matching of RUH with the transducer has not been mentioned yet. The impedance mismatch could cause that the machining process cannot be accurately online monitored by the RUH's impedance. A novel primary side compensation method to achieve both the resonant frequency and impedance matching between the RUH and ultrasonic transducer is proposed in this paper to get same electrical performance as the conventional contact type structure such as electrical brush or slip ring system.

This paper is organized as follows: In Section II, the equivalent circuit of RUH is established to analyze its impedance characteristics. In Section III, the primary series compensation topology is proposed to improve the voltage gain and the output active power capability of the RUH vibrating system. The impedance matching method is applied to RUH vibrating system. In addition, the state-space matrixes are calculated to analyze the voltage response of RUH vibrating system. Section IV presents the experiment verification for the proposed compensation method. Conclusions are presented in Section V.

II. IMPEDANCE MODELLING

A. MECHANICAL STRUCTURE OF RUM

Fig. 1 shows a schematic of the RUH vibrating system, which mainly consists of the power supply, rotary transformer and ultrasonic transducer. The power supply includes the microprocessor, the direct digital synthesizer (DDS) model, a high-power amplifier, the signal sample circuit and compensation elements. A pair of rotary transformers are constructed by winding the copper coils into a ferrite pot core. The primary side and the secondary side are concentrically facing each other. The epoxy resin material is applied to fix copper coils. The magnetic flux provides a mutual inductance that couples ultrasonic energy from the primary to secondary through the air gap. The secondary side and the transducer form the dynamic part of RUH, which rotates with the spindle. The ultrasonic transducer is composed of piezoelectric ceramic stacks, horn, front and back slabs, clamping nut and machining tool. The piezoelectric ceramic stack is a certain material that converts electric power into the mechanical vibration. The vibration amplitude is amplified by the horn. Typically, there are two vibration modes, longitudinal and torsional vibration, which are transferred to machining tool for drilling and grinding [20], [21]. The RUH vibrating system is sensitive to the process force. When the machining tool bumps against a barrier that is difficult to cut, the RUM control system can automatically adjust the feed rate and vibration amplitude of the RUH by the impedance monitoring subsystem to avoid the damage of the RUM system and the processed subject.

The impedance model of the RUH is established by the equivalent circuit [22], [23]. Where C_0 is static capacitance, L_1 is dynamic inductance, C_1 is dynamic capacitance and R_1 is dynamic resistance of ultrasonic transducer. R_L represents

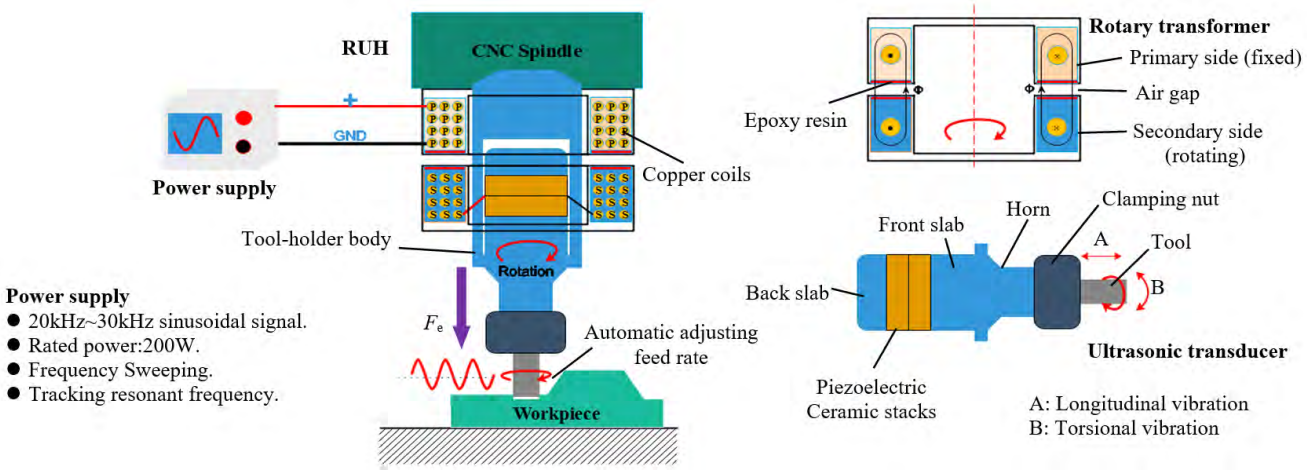

FIGURE 1. RUH configuration.

TABLE 1. Equivalent circuit and impedance expression of RUH.

Parts	Equivalent circuit	Parameters
Ultrasonic transducer	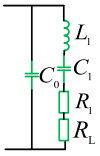	Impedance: $Z_t(\omega)=\dfrac{(\omega^2 L_1C_1-1)-j\omega C_1(R_1+R_L)}{\omega^2 C_0C_1(R_1+R_L)+j[\omega^3 L_1C_1C_0-\omega(C_1+C_0)]}=R_t(\omega)+jX_t(\omega)$ Phase: $\theta_t(\omega)=\tan^{-1}(X_t(\omega)/R_t(\omega))$ Resonant frequency: $f_t=\dfrac{1}{2\pi}\sqrt{\dfrac{(2L_1C_0+L_1C_1-C_0C_1R_1^2)-\sqrt{C_1^2(L_1-C_0R_1^2)^2-4L_1C_1C_0^2R_1^2}}{2L_1^2C_0C_1}}$
Contactless rotary transformer	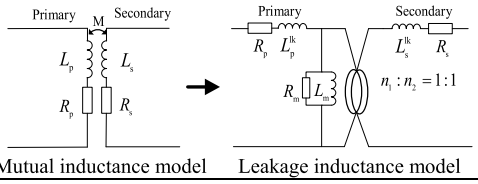	Coils ratio: $n_1:n_2$=50:50=1 Self-inductance: $L_p=L_s$, Mutual inductance:M Magnetization inductance: L_m = M, Magnetization resistance: R_m Leakage inductance: $L_p^{lk}=L_s^{lk}=L_p-M$ Equivalent series resistance: $R_p=R_s$
RUH vibrating system	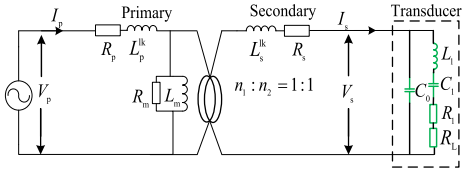	Impedance: $Z_p^n(\omega)=j\omega L_p^{lk}+R_p+\dfrac{Z_m(\omega)\times(j\omega L_s^{lk}+R_s+Z_t(\omega))}{Z_m(\omega)+(j\omega L_s^{lk}+R_s+Z_t(\omega))}=R_p^n(\omega)+jX_p^n(\omega)$, $Z_m(\omega)=\dfrac{j\omega L_mR_m}{j\omega L_m+R_m}$ Phase: $\theta_p^n(\omega)=\tan^{-1}(X_p^n(\omega)/R_p^n(\omega))$ Resonant frequency: f_p (when $X_p^n(\omega)$=0, and $Z_p^n(\omega)$ is the lowest value)

the external equivalent mechanical load. The equivalent circuit of contactless rotary transformer has two types of models, which are the mutual inductance model and leakage inductance model [14], [22]. Using leakage inductance model is easy to obtain the voltage and current response of secondary side, so the leakage inductance model is adopted to analyze the overall behavior of RUH vibrating system.

Based on Thevenin's theory, the impedance, phase and their equivalent parameters of RUH vibrating system can be deduced and summarized in Table 1.

When the ultrasonic transducer operates at the resonant frequency f_t, $\theta_t(\omega) = 0$, $X_t(\omega) = 0$, and $Z_t(\omega)$ reaches to the lowest value. The resonant frequency f_t is the operating frequency of the RUH vibrating system in this study.

TABLE 2. Electrical parameters of ultrasonic transducer.

R_1 (Ω)	C_1 (pF)	C_0 (nF)	L_1 (mH)	f_t (Hz)
78.5931	239.568	2.24419	168.157	25076

B. FREQUENCY AND IMPEDANCE DEVIATIONS

The electrical parameters of rotary transformer and transducer are measured by an impedance analyzer. The results are listed in Table 2 and displayed in Fig.2.

Fig.2 shows the self-inductance value, leakage inductance and equivalent series resistance (ESR) of contactless rotary transformer (coil turns $n_1 = n_2 = 50$) by the impedance analyzer testing. The results show that as the air gap length increases from 0 to 2 mm, the self-inductance and ESR

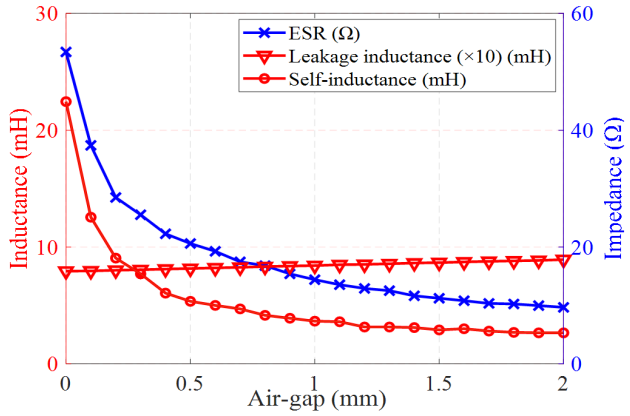

FIGURE 2. Equivalent parameters of rotary transformer.

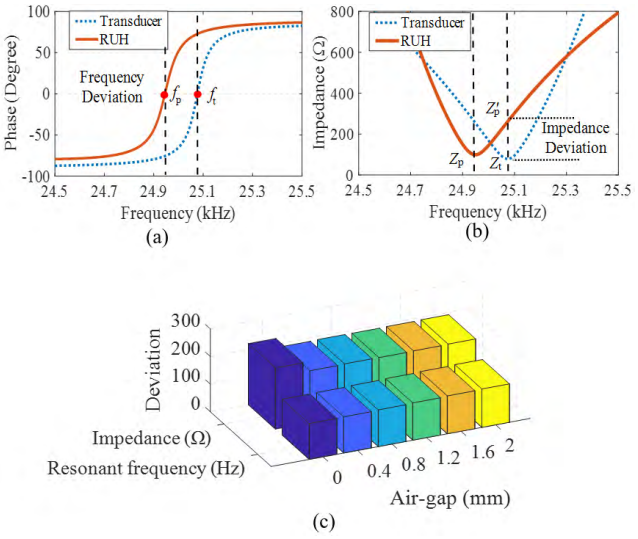

FIGURE 3. Resonant frequency and impedance deviation. (a) Frequency deviation; (b) Impedance deviation; (c) Deviation distribution with different air-gap length.

decrease exponentially. The value of leakage inductance linearly goes up as the air-gap length increases.

The frequency and impedance of the RUH and the ultrasonic transducer are shown in Fig.3, which indicates that there exists resonant frequency and impedance deviations between the RUH and the transducer. Moreover, it is observed that when the air-gap length varies, the resonant frequency and impedance deviations still exist. These deviations would cause the RUH vibrates at non-resonant frequency, and the impedance of transducer cannot be detected accurately by the input impedance of the RUH vibrating system.

III. UNILATERAL COMPENSATION IN PRIMARY SIDE

A. UNILATERAL COMPENSATION IN PRIMARY SIDE

To compensate the frequency and impedance deviations between the RUH and transducer, two typical unilateral

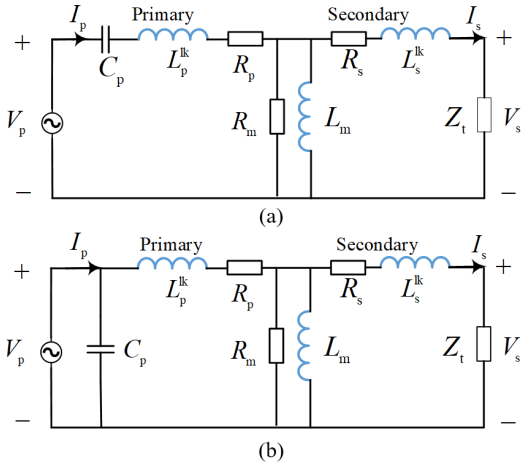

FIGURE 4. Unilateral compensation topology in primary side. (a) P-S; (b) P-P.

TABLE 3. Imepdance and phase of RUH.

P-S	$Z_p^{P\text{-}S}(\omega) = \frac{1}{j\omega C_p} + j\omega L_p^{lk} + R_p + \frac{Z_m(\omega)\times(j\omega L_s^{lk} + R_s + Z_t(\omega))}{Z_m(\omega) + (j\omega L_s^{lk} + R_s + Z_t(\omega))}$ $= R_p^{P\text{-}S}(\omega) + jX_p^{P\text{-}S}(\omega)$ $\theta_p^{p\text{-}s} = \tan^{-1}(X_p^{p\text{-}s}(\omega) / R_p^{p\text{-}s}(\omega))$
P-P	$Z_p^{P\text{-}P}(\omega) = \frac{(j\omega L_p^{lk} + R_p + \frac{Z_m(\omega)\times(j\omega L_s^{lk} + R_s + Z_t(\omega))}{Z_m(\omega) + (j\omega L_s^{lk} + R_s + Z_t(\omega))})}{1 + j\omega C_p(j\omega L_p^{lk} + R_p + \frac{Z_m(\omega)\times(j\omega L_s^{lk} + R_s + Z_t(\omega))}{Z_m(\omega) + (j\omega L_s^{lk} + R_s + Z_t(\omega))})}$ $= R_p^{P\text{-}P}(\omega) + jX_p^{P\text{-}P}(\omega)$ $\theta_p^{p\text{-}p} = \tan^{-1}(X_p^{p\text{-}p}(\omega) / R_p^{p\text{-}p}(\omega))$

topologies (Primary-Series (P-S) topology and Primary-Parallel (P-P) topology), shown in Fig. 4 are studied in this paper.

The impedance and phase expressions of RUH with P-S and P-P topologies are deduced and summarized in Table 3.

When no compensation (NC) is utilized, the real part and imaginary part of RUH at f_t are

$$\mathrm{NC}: \begin{cases} R_p^n(\omega_t) \\ = \dfrac{\left[\begin{array}{l}\omega_t^2 L_m^2(R_t + R_s) \\ +R_p((R_t + R_s)^2 + (\omega_t L_s^{lk} + \omega_t L_m)^2)\end{array}\right]}{(R_t + R_s)^2 + (\omega_t L_s^{lk} + \omega_t L_m)^2} \\ X_p^n(\omega_t) \\ = \dfrac{\left[\begin{array}{l}\omega_t L_m((R_t + R_s)^2 + (\omega_t L_s^{lk})^2 + \omega_t^2 L_m L_s^{lk}) \\ +\omega_t L_p^{lk}((R_t + R_s)^2 + (\omega_t L_s^{lk} + \omega_t L_m)^2)\end{array}\right]}{(R_t + R_s)^2 + (\omega_t L_s^{lk} + \omega_t L_m)^2} \end{cases} \quad (1)$$

where $\omega_t = 2\pi f_t$. When the P-S compensation topology is applied, the real part and imaginary part of RUH at f_t are

TABLE 4. Voltage gain, transfer efficiency and output active power.

NC	Voltage gain	$G_{\mathrm{V}}^{\mathrm{n}}(\omega)=\dfrac{V_{\mathrm{s}}(\omega)}{V_{\mathrm{p}}(\omega)}=\left\lvert\dfrac{Z_{\mathrm{m}}(\omega)\times Z_{\mathrm{t}}(\omega)}{Z_{\mathrm{m}}(\omega)\times(j\omega L_{\mathrm{p}}^{\mathrm{lk}}+R_{\mathrm{p}})+(Z_{\mathrm{m}}(\omega)+j\omega L_{\mathrm{p}}^{\mathrm{lk}}+R_{\mathrm{p}})\times(Z_{\mathrm{t}}(\omega)+j\omega L_{\mathrm{s}}^{\mathrm{lk}}+R_{\mathrm{s}})}\right\rvert$
	Transfer efficiency	$\eta^{\mathrm{n}}(\omega)=\dfrac{I_{\mathrm{s}}^2(\omega)\times R_{\mathrm{t}}(\omega)}{I_{\mathrm{p}}^2(\omega)\times R_{\mathrm{p}}^{\mathrm{n}}(\omega)}=\dfrac{(V_{\mathrm{s}}(\omega)\times Z_{\mathrm{p}}^{\mathrm{n}}(\omega))^2\times R_{\mathrm{t}}(\omega)}{(V_{\mathrm{p}}(\omega)\times Z_{\mathrm{t}}(\omega))^2\times R_{\mathrm{p}}^{\mathrm{n}}(\omega)}$
	Output active power	$P_{\mathrm{out}}^{\mathrm{n}}(\omega)=\dfrac{Z_{\mathrm{m}}^2(\omega)\times Z_{\mathrm{t}}^2(\omega)\times V_{\mathrm{p}}^2}{R_{\mathrm{t}}(\omega)\times(Z_{\mathrm{m}}(\omega)\times(j\omega L_{\mathrm{p}}^{\mathrm{lk}}+R_{\mathrm{p}})+(Z_{\mathrm{m}}(\omega)+j\omega L_{\mathrm{p}}^{\mathrm{lk}}+R_{\mathrm{p}})\times(Z_{\mathrm{t}}(\omega)+j\omega L_{\mathrm{s}}^{\mathrm{lk}}+R_{\mathrm{s}}))^2}$
P-S	Voltage gain	$G_{\mathrm{V}}^{\mathrm{p\text{-}s}}(\omega)=\dfrac{V_{\mathrm{s}}(\omega)}{V_{\mathrm{p}}(\omega)}=\left\lvert\dfrac{Z_{\mathrm{m}}(\omega)\times Z_{\mathrm{t}}(\omega)}{Z_{\mathrm{m}}(\omega)\times(j\omega L_{\mathrm{p}}^{\mathrm{lk}}+R_{\mathrm{p}}+1/(j\omega C_{\mathrm{p}}))+(Z_{\mathrm{m}}(\omega)+j\omega L_{\mathrm{p}}^{\mathrm{lk}}+R_{\mathrm{p}}+1/(j\omega C_{\mathrm{p}}))\times(Z_{\mathrm{t}}(\omega)+j\omega L_{\mathrm{s}}^{\mathrm{lk}}+R_{\mathrm{s}})}\right\rvert$
	Transfer efficiency	$\eta^{\mathrm{p\text{-}s}}(\omega)=\dfrac{I_{\mathrm{s}}^2(\omega)\times R_{\mathrm{t}}(\omega)}{I_{\mathrm{p}}^2(\omega)\times R_{\mathrm{p}}^{\mathrm{p\text{-}s}}(\omega)}=\dfrac{(V_{\mathrm{s}}(\omega)\times Z_{\mathrm{p}}^{\mathrm{p\text{-}s}}(\omega))^2\times R_{\mathrm{t}}(\omega)}{(V_{\mathrm{p}}(\omega)\times Z_{\mathrm{t}}(\omega))^2\times R_{\mathrm{p}}^{\mathrm{p\text{-}s}}(\omega)}$
	Output active power	$P_{\mathrm{out}}^{\mathrm{p\text{-}s}}(\omega)=\dfrac{Z_{\mathrm{m}}^2(\omega)\times Z_{\mathrm{t}}^2(\omega)\times V_{\mathrm{p}}^2}{R_{\mathrm{t}}(\omega)\times(Z_{\mathrm{m}}(\omega)\times(j\omega L_{\mathrm{p}}^{\mathrm{lk}}+R_{\mathrm{p}}+1/(j\omega C_{\mathrm{p}}))+(Z_{\mathrm{m}}(\omega)+j\omega L_{\mathrm{p}}^{\mathrm{lk}}+R_{\mathrm{p}}+1/(j\omega C_{\mathrm{p}}))\times(Z_{\mathrm{t}}(\omega)+j\omega L_{\mathrm{s}}^{\mathrm{lk}}+R_{\mathrm{s}}))^2}$
P-P	Voltage gain	$G_{\mathrm{V}}^{\mathrm{p\text{-}p}}(\omega)=\dfrac{V_{\mathrm{s}}(\omega)}{V_{\mathrm{p}}(\omega)}=\left\lvert\dfrac{Z_{\mathrm{m}}(\omega)\times Z_{\mathrm{t}}(\omega)}{Z_{\mathrm{m}}(\omega)\times(j\omega L_{\mathrm{p}}^{\mathrm{lk}}+R_{\mathrm{p}})+(Z_{\mathrm{m}}(\omega)+j\omega L_{\mathrm{p}}^{\mathrm{lk}}+R_{\mathrm{p}})\times(Z_{\mathrm{t}}(\omega)+j\omega L_{\mathrm{s}}^{\mathrm{lk}}+R_{\mathrm{s}})}\right\rvert$
	Transfer efficiency	$\eta^{\mathrm{p\text{-}p}}(\omega)=\dfrac{I_{\mathrm{s}}^2(\omega)\times R_{\mathrm{t}}(\omega)}{I_{\mathrm{p}}^2(\omega)\times R_{\mathrm{p}}^{\mathrm{p\text{-}p}}(\omega)}=\dfrac{(V_{\mathrm{s}}(\omega)\times Z_{\mathrm{p}}^{\mathrm{p\text{-}p}}(\omega))^2\times R_{\mathrm{t}}(\omega)}{(V_{\mathrm{p}}(\omega)\times Z_{\mathrm{t}}(\omega))^2\times R_{\mathrm{p}}^{\mathrm{p\text{-}p}}(\omega)}$
	Output active power	$P_{\mathrm{out}}^{\mathrm{p\text{-}p}}(\omega)=\dfrac{Z_{\mathrm{m}}^2(\omega)\times Z_{\mathrm{t}}^2(\omega)\times V_{\mathrm{p}}^2}{R_{\mathrm{t}}(\omega)\times(Z_{\mathrm{m}}(\omega)\times(j\omega L_{\mathrm{p}}^{\mathrm{lk}}+R_{\mathrm{p}})+(Z_{\mathrm{m}}(\omega)+j\omega L_{\mathrm{p}}^{\mathrm{lk}}+R_{\mathrm{p}})(Z_{\mathrm{t}}(\omega)+j\omega L_{\mathrm{s}}^{\mathrm{lk}}+R_{\mathrm{s}}))^2}$

calculated as

$$\text{P-S}:\begin{cases}R_{\mathrm{p}}^{\mathrm{p\text{-}s}}(\omega_{\mathrm{t}})\\ \quad=\dfrac{\left[\begin{array}{l}\omega_{\mathrm{t}}^2L_{\mathrm{m}}^2(R_{\mathrm{t}}+R_{\mathrm{s}})+R_{\mathrm{p}}((R_1+R_{\mathrm{s}})^2\\ +(\omega_{\mathrm{t}}L_{\mathrm{s}}^{\mathrm{lk}}+\omega_{\mathrm{t}}L_{\mathrm{m}})^2)\end{array}\right]}{(R_1+R_{\mathrm{s}})^2+(\omega_{\mathrm{t}}L_{\mathrm{s}}^{\mathrm{lk}}+\omega_{\mathrm{t}}L_{\mathrm{m}})^2}\\ X_{\mathrm{p}}^{\mathrm{p\text{-}s}}(\omega_{\mathrm{t}})\\ \quad=\dfrac{\left[\begin{array}{l}(-1/(\omega_{\mathrm{t}}C_{\mathrm{p}}))\times((R_{\mathrm{t}}+R_{\mathrm{s}})^2+(\omega_{\mathrm{t}}L_{\mathrm{s}}^{\mathrm{lk}}+\omega_{\mathrm{t}}L_{\mathrm{m}})^2)\\ +\omega_{\mathrm{t}}L_{\mathrm{m}}((R_{\mathrm{t}}+R_{\mathrm{s}})^2+(\omega_{\mathrm{t}}L_{\mathrm{s}}^{\mathrm{lk}})^2+\omega_{\mathrm{t}}^2L_{\mathrm{m}}L_{\mathrm{s}}^{\mathrm{lk}})\\ +\omega_{\mathrm{t}}L_{\mathrm{p}}^{\mathrm{lk}}((R_{\mathrm{t}}+R_{\mathrm{s}})^2+(\omega_{\mathrm{t}}L_{\mathrm{s}}^{\mathrm{lk}}+\omega_{\mathrm{t}}L_{\mathrm{m}})^2)\end{array}\right]}{(R_{\mathrm{t}}+R_{\mathrm{s}})^2+(\omega_{\mathrm{t}}L_{\mathrm{s}}^{\mathrm{lk}}+\omega_{\mathrm{t}}L_{\mathrm{m}})^2}\end{cases}\tag{2}$$

Similarly, with P-P topology, the real part and imaginary part of RUH's impedance at f_{t} are

$$\text{P-P}:\begin{cases}R_{\mathrm{p}}^{\mathrm{p\text{-}p}}(\omega_{\mathrm{t}})\\ \quad=\dfrac{R_{\mathrm{p}}^{\mathrm{n}}(\omega_{\mathrm{t}})}{(1-\omega_{\mathrm{t}}C_{\mathrm{p}}X_{\mathrm{p}}^{\mathrm{n}}(\omega_{\mathrm{t}}))^2+\omega_{\mathrm{t}}^2C_{\mathrm{p}}^2(R_{\mathrm{p}}^{\mathrm{n}}(\omega_{\mathrm{t}}))^2}\\ X_{\mathrm{p}}^{\mathrm{p\text{-}p}}(\omega_{\mathrm{t}})\\ \quad=\dfrac{X_{\mathrm{p}}^{\mathrm{n}}(\omega_{\mathrm{t}})-\omega_{\mathrm{t}}C_{\mathrm{p}}(R_{\mathrm{p}}^{\mathrm{n}}(\omega_{\mathrm{t}}))^2-\omega_{\mathrm{t}}C_{\mathrm{p}}(X_{\mathrm{p}}^{\mathrm{n}}(\omega_{\mathrm{t}}))^2}{(1-\omega_{\mathrm{t}}C_{\mathrm{p}}X_{\mathrm{p}}^{\mathrm{n}}(\omega_{\mathrm{t}}))^2+\omega_{\mathrm{t}}^2C_{\mathrm{p}}^2(R_{\mathrm{p}}^{\mathrm{n}}(\omega_{\mathrm{t}}))^2}\end{cases}\tag{3}$$

When $X_{\mathrm{p}}^{\mathrm{p\text{-}s}}(\omega_{\mathrm{t}})=0$, the series capacitance value is

$$C_{\mathrm{p}}^{\mathrm{p\text{-}s}}=\frac{((R_{\mathrm{t}}+R_{\mathrm{s}})^2+(\omega_{\mathrm{t}}L_{\mathrm{s}}^{\mathrm{lk}}+\omega_{\mathrm{t}}L_{\mathrm{m}})^2)}{\left[\begin{array}{l}\omega_{\mathrm{t}}^2L_{\mathrm{m}}((R_{\mathrm{t}}+R_{\mathrm{s}})^2+(\omega_{\mathrm{t}}L_{\mathrm{s}}^{\mathrm{lk}})^2+\omega_{\mathrm{t}}^2L_{\mathrm{m}}L_{\mathrm{s}}^{\mathrm{lk}})\\ +\omega_{\mathrm{t}}^2L_{\mathrm{p}}^{\mathrm{lk}}((R_{\mathrm{t}}+R_{\mathrm{s}})^2+(\omega_{\mathrm{t}}L_{\mathrm{s}}^{\mathrm{lk}}+\omega_{\mathrm{t}}L_{\mathrm{m}})^2)\end{array}\right]}\tag{4}$$

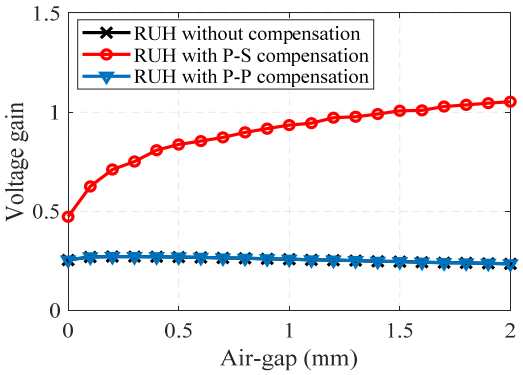

FIGURE 5. Voltage gain with different air-gap length.

When $X_{\mathrm{p}}^{\mathrm{p\text{-}p}}(\omega_{\mathrm{t}})=0$, the parallel capacitance value is

$$C_{\mathrm{p}}^{\mathrm{p\text{-}p}}=\frac{X_{\mathrm{p}}^{\mathrm{n}}(\omega_{\mathrm{t}})}{\omega_{\mathrm{t}}((R_{\mathrm{p}}^{\mathrm{n}}(\omega_{\mathrm{t}}))^2+(X_{\mathrm{p}}^{\mathrm{n}}(\omega_{\mathrm{t}}))^2)}\tag{5}$$

The expressions of voltage gain, power transfer efficiency and output active power of RUH with NC, P-S and P-P compensation topologies are deduced and summarized in Table 4.

B. VOLTAGE GAIN AND TRANSFER EFFICIENCY

Based on the parameters in Table 2, (4), (5) and the Table 4, the voltage gains of RUH vibrating system with the NC, P-S and P-P topologies are calculated and shown in Fig.5. It is found that when the RUH is without any

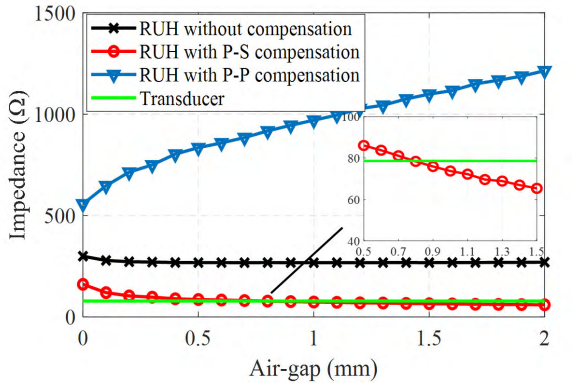

FIGURE 6. Input impedance with different air-gap length.

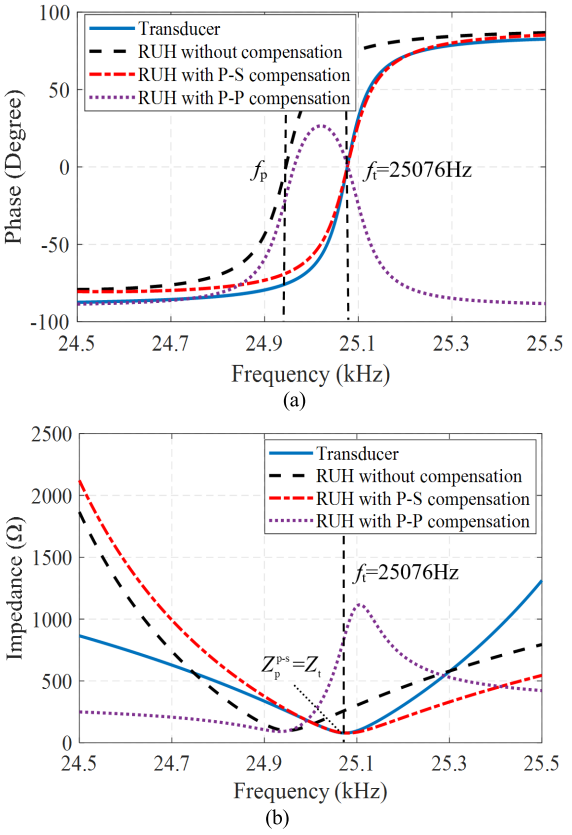

FIGURE 7. Resonant frequency and impedance compensation. (a) Resonant frequency compensation; (b) Impedance compensation.

compensation elements, the voltage gain of the rotary transformer is much smaller than 1. When the P-S topology is applied to the RUH vibrating system, the voltage gain increases with the augment of air-gap length in a certain range. However, the P-P topology barely improves the voltage gain of RUH vibrating system.

In Fig. 6, it shows that by adjusting the air-gap length, only with P-S topology the impedance of RUH can match with the impedance of the transducer (the intersection appears when the air-gap length is 0.8mm). When the air-gap length is 0.8mm, the self-inductance, leakage inductance and ESR of contactless rotary transformer are 8.40mH, 0.832mH and 8.3Ω, respectively.

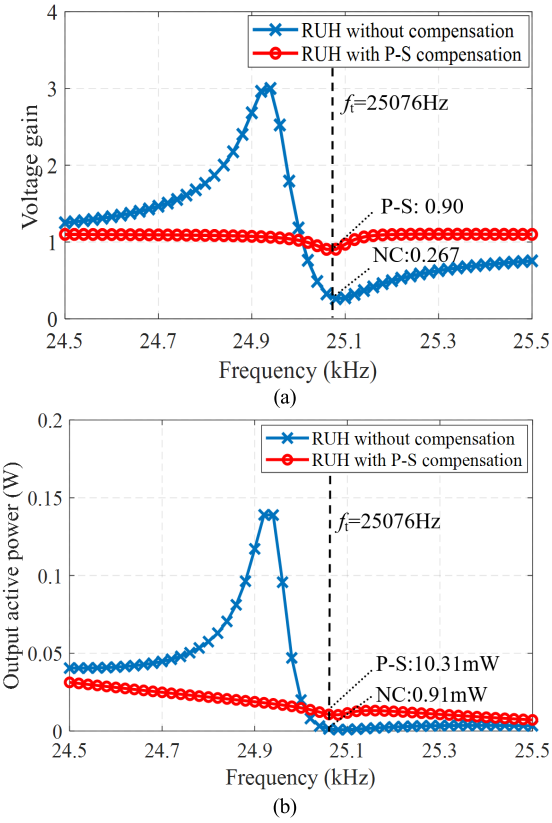

FIGURE 8. Voltage gain and output active power with and without compensation. (a) Voltage gain; (b) Output active power.

The compensation result with 0.8mm air-gap is verified and visualized in Fig.7. It is found that although the resonant frequency deviation can be eliminated by the P-S and P-P topologies at resonant frequency f_t, the impedance of RUH can only be matched with the one of the transducer by P-S topology. Based on above analysis, the P-S topology is chosen as the compensation topology for the RUH vibrating system in our study.

The voltage gain and output active power of the RUH vibrating system with NC and P-S topologies in frequency sweeping are shown in Fig.8. It is observed that compared with NC topology the P-S topology improves voltage gain from 0.267 to 0.90 at $f_t = 25076$ Hz. Moreover, it is found that the voltage gain with P-S topology is more stable than the voltage gain without compensation topology during frequency sweeping. To analyze the output active power capability, the input effective voltage is set as 1V, the output active powers of two topologies are calculated according to equations in Table 4. The result is shown in Fig. 8 (b) and it is found that the output active power with P-S topology is 11.3 times than the one without any compensation.

Mechanical load is an important factor affecting the dynamics of the RUH vibrating system. The voltage gain, output active power and power transfer efficiency with different mechanical load are shown in Fig.9. It is observed that the voltage gain and output active power with P-S compensation is always greater than the one with NC topology

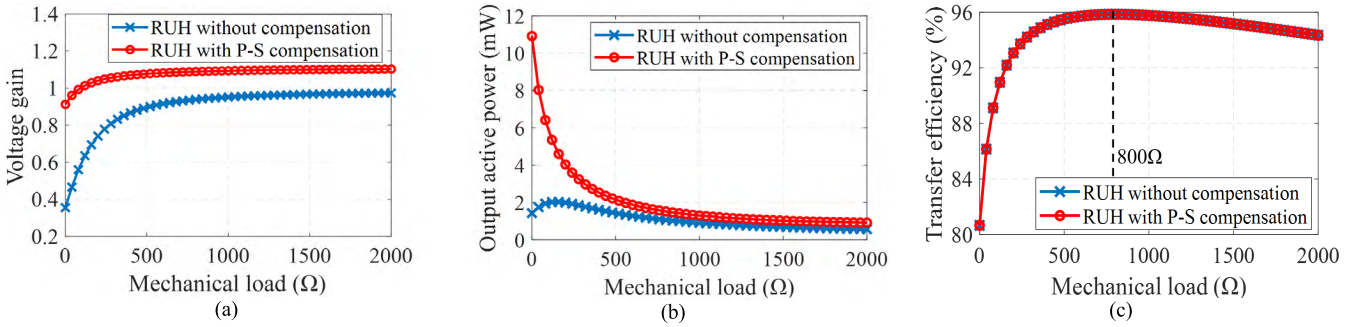

FIGURE 9. Voltage gain, output active power and power transfer efficiency with different mechanical load. (a) Voltage gain; (b) Output active power; (c) Power transfer efficiency.

TABLE 5. The coefficient and input matrix.

RUH (i=1)

$$A_1=\begin{bmatrix} -\frac{R_p+R_m}{L_p^{lk}} & \frac{R_m}{L_p^{lk}} & \frac{R_m}{L_p^{lk}} & 0 & 0 & 0 \\ \frac{R_m}{L_m} & -\frac{R_m}{L_m} & -\frac{R_m}{L_m} & 0 & 0 & 0 \\ \frac{R_m}{L_s^{lk}} & -\frac{R_m}{L_s^{lk}} & -\frac{R_m+R_s}{L_s^{lk}} & -\frac{1}{L_s^{lk}} & 0 & 0 \\ 0 & 0 & \frac{1}{C_0} & 0 & -\frac{1}{C_0} & 0 \\ 0 & 0 & 0 & \frac{1}{L_1} & -\frac{R_1}{L_1} & -\frac{1}{L_1} \\ 0 & 0 & 0 & 0 & \frac{1}{C_1} & 0 \end{bmatrix} \quad B_1=\begin{bmatrix} \frac{1}{L_p^{lk}} \\ 0 \\ 0 \\ 0 \\ 0 \\ 0 \end{bmatrix} \quad C_1=\begin{bmatrix} 0&0&0&0&0&0 \\ 0&0&0&0&0&0 \\ 0&0&1&0&0&0 \\ 0&0&0&1&0&0 \\ 0&0&0&0&0&0 \\ 0&0&0&0&0&0 \end{bmatrix} \quad x_1=\begin{bmatrix} i_{L_p}(t) \\ i_{L_m}(t) \\ i_{L_s}(t) \\ u_s(t) \\ i_{L_1}(t) \\ u_{C_1}(t) \end{bmatrix}$$

RUH with P-S topology (i=2)

$$A_2=\begin{bmatrix} 0 & \frac{1}{C_p} & 0 & 0 & 0 & 0 & 0 \\ -\frac{1}{L_p^{lk}} & -\frac{R_p+R_m}{L_p^{lk}} & \frac{R_m}{L_p^{lk}} & \frac{R_m}{L_p^{lk}} & 0 & 0 & 0 \\ 0 & \frac{R_m}{L_m} & -\frac{R_m}{L_m} & -\frac{R_m}{L_m} & 0 & 0 & 0 \\ 0 & \frac{R_m}{L_s^{lk}} & -\frac{R_m}{L_s^{lk}} & -\frac{R_m+R_s}{L_s^{lk}} & -\frac{1}{L_s^{lk}} & 0 & 0 \\ 0 & 0 & 0 & \frac{1}{C_0} & 0 & -\frac{1}{C_0} & 0 \\ 0 & 0 & 0 & 0 & \frac{1}{L_1} & -\frac{R_1}{L_1} & -\frac{1}{L_1} \\ 0 & 0 & 0 & 0 & 0 & \frac{1}{C_1} & 0 \end{bmatrix} \quad B_2=\begin{bmatrix} 0 \\ \frac{1}{L_p^{lk}} \\ 0 \\ 0 \\ 0 \\ 0 \\ 0 \end{bmatrix} \quad C_2=\begin{bmatrix} 0&0&0&0&0&0&0 \\ 0&0&0&0&0&0&0 \\ 0&0&0&0&0&0&0 \\ 0&0&0&1&0&0&0 \\ 0&0&0&0&1&0&0 \\ 0&0&0&0&0&0&0 \\ 0&0&0&0&0&0&0 \end{bmatrix} \quad x_2=\begin{bmatrix} u_{C_p}(t) \\ i_{L_p}(t) \\ i_{L_m}(t) \\ i_{L_s}(t) \\ u_s(t) \\ i_{L_1}(t) \\ u_{C_1}(t) \end{bmatrix}$$

when mechanical load changes. The output active powers of NC and P-S topologies decrease exponentially as the load increases (Fig. 9(b)). The power transfer efficiency reaches to its maximum value 95.85% with 800Ω mechanical load in Fig.9 (c). It is found that the power transfer efficiencies of NC and P-S topologies are identical with different mechanical loads.

C. RESPONSE ANALYSIS

In this paper, the frequency and impedance deviations of RUH vibrating system are compensated by the P-S topology. The state-space equation of RUH vibrating system is

$$\begin{aligned} \dot{x}_i &= A_i x_i + B_i u \\ y &= C_i x_i \end{aligned} \tag{6}$$

where the output $y = [V_s(t), I_s(t)]^T$, the $u = V_p(t) = 1\times\sin(2\pi f_t)$, and the coefficient and input matrix are listed in Table 5.

In Table 5, $V_{Cp}(t)$ is the voltage of C_p. $I_p(t)$ and $I_s(t)$ are the input currents of the RUH and the ultrasonic transducer, respectively. $I_m(t)$ is the current of L_m, $V_s(t)$ is the voltage of the ultrasonic transducer. $I_{L_1}(t)$ is the current of equivalent dynamic inductance and $V_{C_1}(t)$ is the voltage of equivalent dynamic capacitance.

The output voltage response of RUH vibrating system is shown in Fig.10. The output voltage of the RUH without any compensations oscillates at initial 15ms (Fig.10 (a)). However, the output voltage of RUH with P-S topology is stable and can achieve greater value than that of NC topology

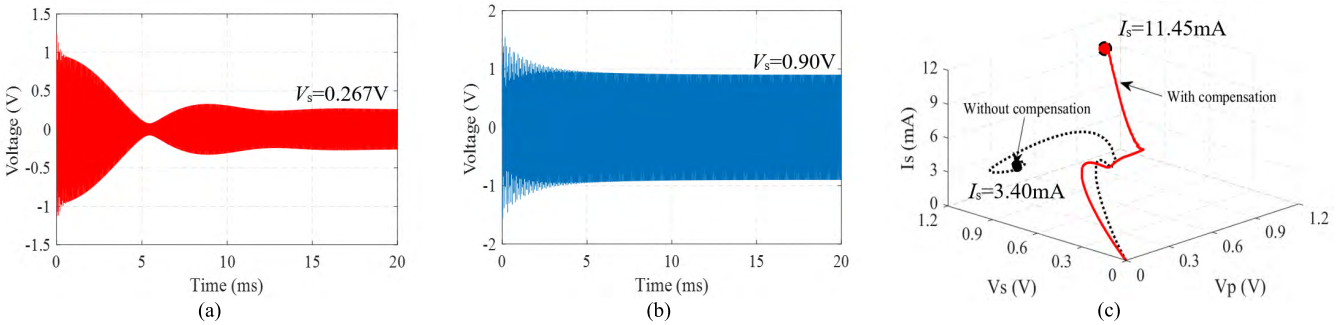

FIGURE 10. Voltage and current response of RUH. (a) Voltage response without compensation; (b) Voltage response with compensation; (c) 3D perspective response.

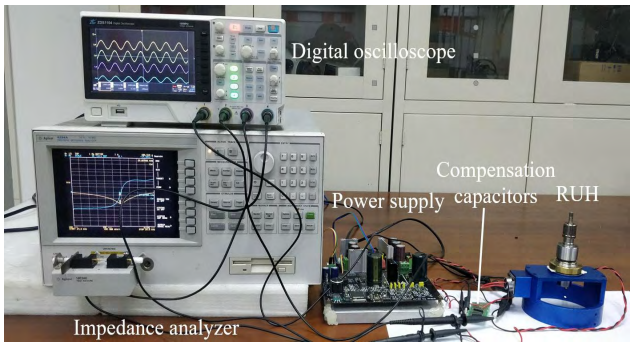

FIGURE 11. Experimental platform.

at initialization time (Fig.10 (b)). Fig.10 (c) demonstrates the output current trajectory when the system is in initialization period. The current of the ultrasonic transducer without any compensations is lower than that with the compensation elements at steady-state. It indicates that the RUH vibrating system with P-S compensation can transmit more active power from the primary side to secondary side of RUH vibrating system.

IV. EXPERIMENT

In Fig.11, an experimental platform is built to verify the impedance model of RUH, and the performance of the proposed compensation method. A self-developed RUH and ultrasonic power supply are utilized to evaluate the voltage response with and without compensation elements. Frequency and impedance characteristics of RUH and ultrasonic transducer, and the equivalent parameters of contactless rotary transformer are measured by an impedance analyzer (Agilent Model 4294A). All the data is sampled by a digital oscilloscope (ZDS1104).

A. CHARACTERISTICS OF ROTARY TRANSFORMER

The spindle rotary speed has no influence on the compensation performance and stability of the RUH according to [19]. Since the coils of the primary and secondary sides are not wound on the same magnetic core, the electrical characteristics of contactless rotary transformers are sensitive to the length of the air gap. As shown in Fig. 2, when the air gap length gets smaller, the self-inductance value and ESRs of

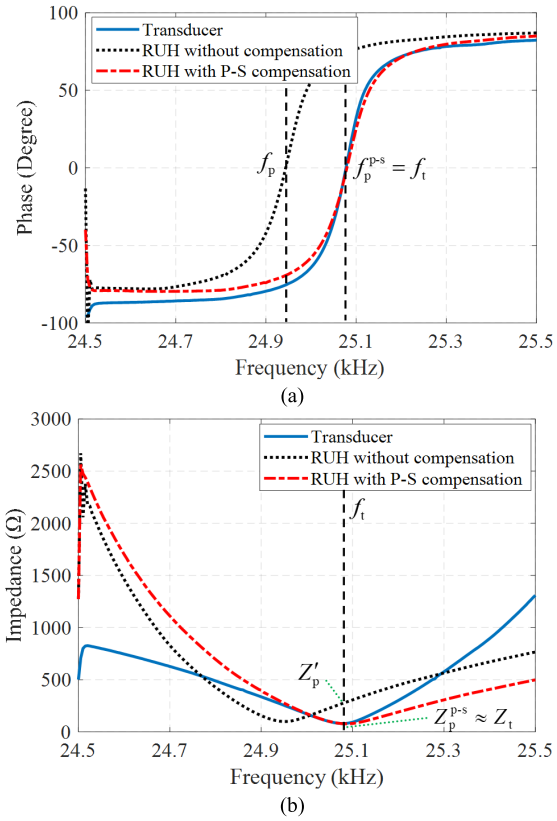

FIGURE 12. Frequency and impedance of the RUH and the transducer. (a) Frequency compensation; (b) Impedance compensation.

the contactless rotary transformer become larger. Its characteristics are quite different from those of the strongly coupled transformer, which the primary and the secondary side coils are concentrically overlapped around the same magnetic core. The ESRs of the tightly inductive-coupled transformer are quite small and they can be neglected, however, the ESRs of contactless rotary transformers need to be considered to solve the impedance matching problem in this study.

B. FREQUENCY AND IMPEDANCE MEASUREMENT

The impedance and frequency of RUH vibrating system measured in the experiment are shown in Fig.12. It is found that there exists the deviations of the resonant frequency and

TABLE 6. Frequency and impedance compensation.

f_t (Hz)	f_p (Hz)	$f_p^{p\text{-}s}$ (Hz)	$Z_t(\Omega)$	$Z_p'(\Omega)$	$Z_p^{p\text{-}s}(\Omega)$
25076	24942	25076	78.6	267.7	78

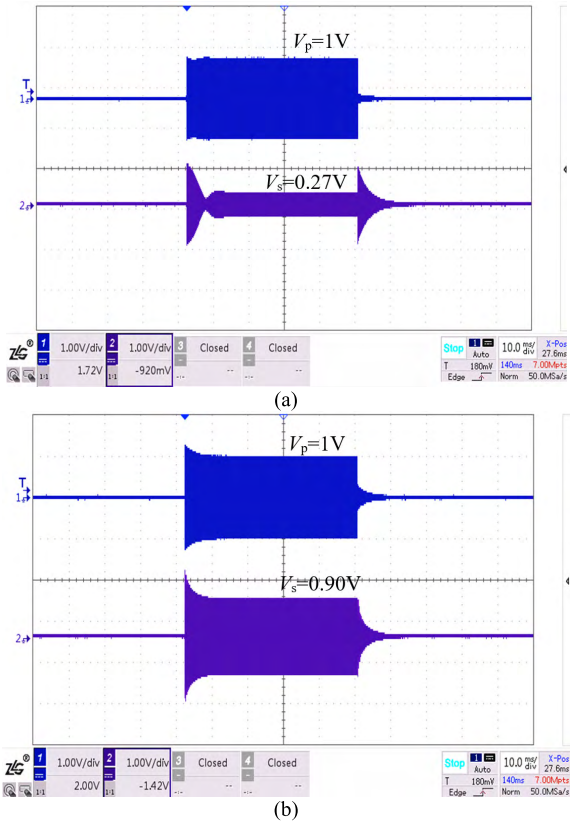

FIGURE 13. Voltage response. (a) No compensation; (b) P-S compensation.

impedance when the RUH vibrating system is without any compensations. While the deviations are eliminated and the resonant frequency is matched well after the P-S topology is applied. The input impedance reaches to 78Ω. The RUH's impedance is compensated by the compensation capacitors at the 0.8mm air-gap. The compensation details are listed in Table 6.

C. THE VOLTAGE TESTING

The voltage responses of the RUH vibrating system with NC and P-S topologies are shown in Fig.13. The input voltage is $V_p = 1$V. With P-S topology, the output voltage response of the RUH rapidly reaches steady-state, but the output voltage without any compensations oscillates in initial time. With the same input voltage, the output voltage with P-S topology can increase from 0.27V to 0.90V during steady-state.

D. THE LOAD TESTING

To verify the monitoring performance with different loads, a group of experiments are conducted to test the input impedance of the RUH at different machining force (F_e)

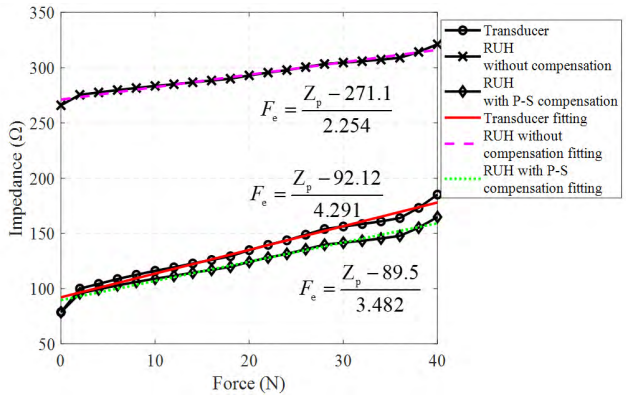

FIGURE 14. Impedances of the RUH and the transducer with the different force.

in Fig.14. The force is pushed vertically to the machining tool, and quantified by a digital force device (model JL-DT01). It is observed that the input impedance of RUH with P-S compensation increases linearly with external force and has a better impedance follow-up trend with the transducer compared to NC topology. It means that the impedance matching between the RUH and the transducer is beneficial to monitor the impedance of the transducer and the machining process in the RUM.

V. CONCLUSIONS

This paper proposes a novel unilateral compensation method to eliminate the resonant frequency and impedance deviations in the RUM. This proposed method is easy to implement and maintain in the industry application. The conclusions are drawn as follows:

1) Due to the leakage inductance and ESRs of the contactless rotary transformer, the resonance frequency of the RUH deviates from the ultrasonic transducer, which causes the RUH vibrating system to be unstable and with low output power.

2) The P-S and P-P compensation topologies are applied and analyzed. It is found that with P-S unilateral compensation method the output voltage responses quickly, the voltage gain increases from 0.267 to 0.90, and the output active power is enhanced by 11.3 times compared to the one without any compensation methods.

3) The voltage gain, output active power and input impedance of the RUH vary with the length of the air-gap of rotary transformer. By adjusting the length of the air-gap, the input impedance of RUH with P-S unilateral compensation can match with the impedance of the ultrasonic transducer.

4) The experimental results validate the effectiveness of the proposed method. It shows that the proposed method can accurately match both the resonant frequency and impedance of RUH with the ultrasonic transducer. When driven by the resonant frequency, the output voltage of RUH can be optimized to obtain a faster response and a greater value. The impedance monitoring performance is also improved.

REFERENCES

[1] R. P. Singh and S. Singhal, "Rotary ultrasonic machining: A review," *Adv. Manuf. Process.*, vol. 31, no. 14, pp. 1795–1824, 2016.
[2] J. Wang, J. Zhang, P. Feng, and G. Ping, "Damage formation and suppression in rotary ultrasonic machining of hard and brittle materials: A critical review," *Ceramics Int.*, vol. 44, no. 2, pp. 1227–1239, 2018.
[3] M. Zvoncan, M. Beno, M. Kovac, and J. Peterka, "Cross section of machined layer for rotary ultrasonic machining with a hollow drill," *Manuf. Ind. Eng.*, vol. 11, no. 3, pp. 11–13, 2012.
[4] N. Churi, "Rotary ultrasonic machining of hard-to-machine materials," Ph.D. dissertation, Kansas State Univ., Manhattan, KS, USA, 2010.
[5] J. Janghorbanian, M. R. Razfar, and M. M. A. Zarchi, "Effect of cutting speed on tool life in ultrasonic-assisted milling process," *Proc. Inst. Mech. Eng. B, J. Eng. Manuf.*, vol. 227, no. 8, pp. 1157–1164, 2013.
[6] S. B. Bhosale, R. S. Pawade, and P. K. Brahmankar, "Effect of process parameters on MRR, TWR and surface topography in ultrasonic machining of alumina–zirconia ceramic composite," *Ceramics Int.*, vol. 40, no. 8, pp. 12831–12836, Sep. 2014.
[7] X. Tang, Y. Liu, S. Shi, W. Chen, and X. Qi, "Development of a novel ultrasonic drill using longitudinal-bending hybrid mode," *IEEE Access*, vol. 5, pp. 7362–7370, 2017.
[8] Y. Liu, J. Yan, L. Wang, and W. Chen, "A two-DOF ultrasonic motor using a longitudinal–bending hybrid sandwich transducer," *IEEE Trans. Ind. Electron.*, vol. 66, no. 4, pp. 3041–3050, Apr. 2019.
[9] A. Mathieson, A. Cardoni, P. Harkness, and M. Lucas, "Characterisation of nonlinear behaviour of power ultrasonic drilling horns," in *Proc. IEEE Int. Ultrason. Symp.*, vol. 104, no. 3, Sep. 2009, pp. 2092–2095.
[10] S. Ditze, A. Endruschat, T. Schriefer, A. Rosskopf, and T. Heckel, "Inductive power transfer system with a rotary transformer for contactless energy transfer on rotating applications," in *Proc. IEEE Int. Symp. Circuits Syst.*, Montreal, QC, Canada, May 2016, pp. 1622–1625.
[11] W. Cai, J. Zhang, P. Feng, D. Yu, and Z. Wu, "A bilateral capacitance compensation method for giant magnetostriction ultrasonic processing system," *Int. J. Adv. Manuf. Technol.*, vol. 90, nos. 9–12, pp. 2925–2933, 2017.
[12] J. P. C. Smeets, L. Encica, and E. A. Lomonova, "Comparison of winding topologies in a pot core rotating transformer," in *Proc. IEEE 12th Int. Conf. Optim. Elect. Electron. Equip. (OPTIM)*, Basov, Romania, May 2010, pp. 103–110.
[13] D. Bortis, I. Kovacevic, L. Fässler, and J. W. Kolar, "Optimization of rotary transformer for high-speed applications," in *Proc. IEEE 14th Workshop Control Modeling Power Electron.*, Salt Lake City, UT, USA, Jun. 2013, pp. 1–6.
[14] X. Zhu, B. Lin, L. Liu, and Y. Luan, "Power transfer performance and cutting force effects of contactless energy transfer system for rotary ultrasonic grinding," *IEEE Trans. Ind. Electron.*, vol. 63, no. 5, pp. 2785–2795, May 2016.
[15] X. Zhu, B. Lin, and L. Liu, "Efficiency-based compensations and the mechanical load dependencies of rotary transformer for rotary ultrasonic machining applications," *IET Power Electron.*, vol. 8, no. 6, pp. 986–993, Jun. 2015.
[16] J. Imaoka and M. Shoyama, "A leakage flux cancellation technique for series-parallel combined resonant circuits with asymmetric rotary transformers used for ultrasonic spindle drive," in *Proc. Int. Power Electron. Conf.*, May 2018, pp. 1554–1561.
[17] J. Imaoka, M. Nam, M. Shoyama, and H. Fujita, "Design of series-parallel combined resonant circuit with rotary transformer used for ultrasonic spindle drive," in *Proc. IEEE 3rd Int. Future Energy Electron. Conf. ECCE Asia*, Jun. 2017, pp. 2244–2249.
[18] L. Liu, B. Lin, and X. Zhu, "Optimization of rotary transformer for RUM with secondary self-compensation," *AEU-Int. J. Electron. Commun.*, vol. 83, pp. 73–80, Jan. 2018.
[19] X. Jiang, K. Wang, R. Shao, J. K. Mills, and D. Zhang, "Self-compensation theory and design of contactless energy transfer and vibration system for rotary ultrasonic machining," *IEEE Trans. Power Electron.*, vol. 33, no. 10, pp. 8650–8660, Oct. 2018.
[20] Y. X. Liu, J. K. Liu, W. S. Chen, and S. J. Shi, "Actuating mechanism and analysis of a square-type rotary ultrasonic stator using longitudinal vibration transducers," *Appl. Mech. Mater.*, vols. 16–19, pp. 323–327, 2009.
[21] A.-B. Hassan, L. Margaret, and H. Patrick, "A design approach for longitudinal–torsional ultrasonic transducers," *Sens. Actuators A, Phys.*, vol. 198, no. 15, pp. 99–106, 2013.
[22] Y.-H. Kim and K.-H. Jin, "Design and implementation of a rectangular-type contactless transformer," *IEEE Trans. Ind. Electron.*, vol. 58, no. 12, pp. 5380–5384, Dec. 2011.
[23] W. P. Mason, *Electromechanical Transducers and Wave Filters*. Princeton, NJ, USA: Van Nostrand, 1948.

JIANGUO ZHANG received the M.S. degree in control science and engineering from the Harbin Institute of Technology, Harbin, China, in 2012. He is currently pursuing the Ph.D. degree with the Department of Mechatronics, Harbin Institute of Technology (Shenzhen), Shenzhen, China.

His current research interests include the control modeling and optimization of power ultrasonic systems.

ZHILI LONG received the B.S., M.S., and Ph.D. degrees in mechatronics engineering from Central South University, Changsha, China, in 2000, 2002, and 2007, respectively.

He is currently an Associate Professor with the Department of Mechatronics, Harbin Institute of Technology (Shenzhen), Guangdong, China. His research interests include the process analysis of ultrasonic packaging, and the model and optimization of ultrasonic actuators.

CAN WANG (M'15) received the Ph.D. degree in electrical engineering from McGill University, Montreal, Canada, in 2015. In 2016, he was a Research Engineer with the China Southern Grid Electric Power Research Institute. In 2017, he joined the Harbin Institute of Technology, Shenzhen, as an Assistant Professor. His research interests include the modeling, control, and simulation of power electronics converters, and the power grid integration of renewable energies such as wind and solar.

FENG REN received the M.S. degree in control science and engineering from Xi'an Shiyou University, Xi'an, China, in 2017. He is currently an Electronic Engineer with the Department of Mechatronics, Harbin Institute of Technology (Shenzhen), Guangdong, China.

His current research interests include the electric control systems of ultrasonic drivers.

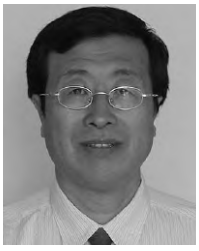

YANGMING LI (M'98–SM'04) received the B.S. and M.S. degrees in mechanical engineering from Jilin University, Changchun, China, in 1985 and 1988, respectively, and the Ph.D. degree in mechanical engineering from Tianjin University, Tianjin, China, in 1994. He is currently a Full Professor with the Department of Industrial and Systems Engineering, The Hong Kong Polytechnic University. His research interests include micro/nanomanipulation, compliant mechanism, precision engineering, robotics, and multibody dynamics and control. He is an Associate Editor of the IEEE TRANSACTIONS AUTOMATIC SCIENCE ENGINEERING, *Mechatronics*, and the *International Journal of Control, Automation, and Systems*.